SLAC-PUB-10845
November 2004

JOURNAL of APPLIED PHYSICS

Microstructural comparisons of ultra-thin Cu films deposited by ion-beam and dc-magnetron sputtering

W. L. Prater[a)] and E. L. Allen
Chemical and Materials Engineering Dept., San Jose State University, One Washington Square, San Jose, California 95192

W. -Y. Lee
Hitachi Global Storage Technologies, 5600 Cottle Road, San Jose, California *95193*

M. F. Toney
Stanford Synchrotron Radiation Laboratory, Stanford Linear Accelerator Center, 2575 Sand Hill Road, Menlo Park, California 94025

A. Kellock, J. S. Daniels[b)], J. A. Hedstrom and T. Harrell[c)]
IBM Almaden Research Center, 650 Harry Road, San Jose, California 95120

a) Electronic mail: masterprater@aol.com Present address: Novellus Systems, Inc., M/S HQ-2C, 4000 North First Street, San Jose, CA 95134
b) Present address: Department of Electrical Engineering, Stanford University, Stanford, CA 94305.
c) Present address: Department of Materials Science and Engineering, University of Virginia, Charlottesville, VA 22903.

We report and contrast both the electrical resistance and the microstructure of copper thin films deposited in an oxygen containing atmosphere by ion-beam and dc-magnetron sputtering. For films with thicknesses 5 nm or less, the resistivity of the Cu films is minimized at oxygen concentrations ranging from 0.2% to 1% for dc-magnetron sputtering and 6% to 10% for ion beam sputtering. Films sputtered under both conditions show a similar decrease of interface roughness with increasing oxygen concentration, although the magnetron deposited films are smoother. The dc-magnetron produced films have higher resistivity, have smaller Cu grains, and contain a higher concentration of cuprous oxide particles. We discuss the mechanisms leading to the grain refinement and the consequent reduced resistivity in both types of films.

Work supported in part by the Department of Energy Contract DE-AC02-76SF00515

I. INTRODUCTION

Recently, magnetic recording areal densities of hard disk drives have increased at a compound annual growth rate of nearly 100%,[1] which has lead to a technology race among the hard-disk-drive companies for the highest sensitivity read heads. The current generation of spin-valve read heads uses the giant magnetoresistance (GMR)[2] effect to sense the magnetic bits on disks. The strength of the GMR effect is, in part, dependent upon the interfacial structure of the multilayer film stack that makes up the sensor, which in turn is dependent upon the film growth. Hence, understanding and controlling thin film growth and properties are vitally important for the magnetic recording industry and, in general, any technology relying on thin films.

One approach to achieve higher sensitivity is the enhancement of GMR through an increase in specular electron scattering at the interfaces in the spin-valve.[1,3,4] This enhancement partially results from an increased mean free path of majority spin-polarized electrons through reflection at interfaces in the spin-valve, which increases GMR ($\Delta R/R$) by increasing ΔR (change in resistance) and/or decreasing the resistance (R). This has been achieved by the counterintuitive approach of introducing impurities in the sputtering chamber during thin film deposition. One such impurity is oxygen. Its effect on the growth and properties of GMR films is only recently being investigated[5-7] and the role of oxygen in increasing GMR is still a matter of debate. Egelhoff *et al.*[8,9] have reported that introducing several parts per million of oxygen during dc-magnetron deposition of Co/Cu spin-valves led to lower resistivity and greater GMR. They proposed a surfactant mechanism in which oxygen impedes interlayer mixing between Co and Cu during film growth, leading to lower ferromagnetic coupling and lower resistance.

Additionally, they propose that the presence of oxygen during sputtering acts to reduce the interface roughness and increase grain size. Miura *et al.*[10] partially oxidized Co/Cu multilayers during dc-magnetron sputtering and found increased GMR and higher antiferromagnetic coupling. Using results from atomic force microscopy, X-ray reflectivity and X-ray diffraction measurements of the films, they proposed a mechanism involving a combination of reduced grain size and decreased interface roughness. They conclude that control of the oxygen concentration is critical to influencing the film microstructure which results in an increase in specular electron scattering and thus enhancement of the GMR. Larson *et al.*[11] introduced 500 to 1450 atomic parts per million of oxygen during growth of dc-magnetron sputtered Cu/CoFe multilayers and found the GMR increased from 1% to 7%. Using an elegant three-dimensional atom probe, they found that oxygen results in reduced interfacial mixing and conformal roughness. Transmission electron microscopy observations showed reduced grain boundary grooving. It is hypothesized that oxygen alters the balance between the surface and the interfacial tensions, thereby reducing grain boundary grooving. Li *et al.*[12] investigated the effect of oxygen on CoFe/Cu spin-valves deposited by ion-beam sputtering by exposing the fresh surface of the newly deposited metal film to pure oxygen for a specific time and at a specific pressure. They found a 10% GMR increase attributed to an increase in the spin-dependent transmission coefficient and suppression of diffuse scattering. Peterson *et al.*[13] introduced oxygen during dc-magnetron sputtering of Co/Cu multilayers. They studied the films with diffuse and specular x-ray reflectivity and found that the oxygen produced smoother films, suppressed pinhole formation, reduced interlayer mixing, and increased the extent to which the roughness was conformal.

Finally, grain size, another factor that can affect resistivity, has been compared between ion-beam and dc-magnetron sputtered spin-valves grown on different seed layers using native SiO_2 for ion-beam deposition and Al_2O_3 and Ta for dc-magnetron deposition. Bailey *et al*. found the grains to be larger and more columnar in the ion-beam films.[14] Prater *et al*. found that low concentrations of oxygen in the sputtering atmosphere reduced grain size, smoothed the interface and reduced the resistivity of ion-beam deposited Cu thin films.[15]

To summarize the previous work, spin-valve GMR and resistivity have been improved by the introduction of oxygen under various concentrations during sputtering and for different film deposition processes. It appears that oxygen favorably alters the film microstructure and smoothes the interfaces, which increases specular scattering of conduction electrons at the interfaces. Some work indicates that oxygen acts as a surfactant floating out on the growing surface,[8,9,11] while Miura *et al*. and Prater *et al*. proposed that the oxygen is incorporated in the film.[10,15] Hence, the mechanism of interface smoothing is still unknown and is, perhaps, dependent on oxygen concentration and film processing.

In this paper we compare the oxygen concentrations needed to reduce the resistivities of Cu films produced by dc-magnetron and ion-beam sputtering and elucidate the compositional and microstructural differences leading to the reduced resistivity. Through a comparison of the interface roughness and specular electron scattering calculated by the Fuchs-Namba model and measured by X-ray reflectivity, we show that the resistivity reduction is due to the formation of smoother interfaces, which increases specular scattering of electrons. The smoother interfaces result from the formation of

small cuprous oxide particles in the Cu films that limit the copper grain growth. Compared to ion-beam films, the dc-magnetron films have larger Cu and Cu_2O grain sizes and have a significantly higher fraction of Cu_2O at O_2 concentrations that produce minimal electrical resistivity.

II. EXPERIMENTAL PROCEDURES

The copper films deposited in the dc-magnetron sputtering system[5] used argon gas mixed with oxygen at a total pressure of 0.4 Pa; the oxygen volumetric percentage was varied from 0% to 3% of the total flow. The base pressure prior to sputtering was 1.3×10^{-5} Pa. Film thickness was controlled by a quartz crystal mass monitor in the chamber that stopped the sputtering at the desired set-point thickness. The dc-magnetron sputtering rate was 0.12 nm/s using a dc-power source at 113 W. The copper films deposited in the ion-beam sputtering system[5] used xenon gas mixed with oxygen at a total flow rate of 0.55 standard cubic centimeters (sccm) at a pressure of 0.012 Pa. The base pressure prior to sputtering was 2.4×10^{-6} Pa. The oxygen volumetric percentage was varied from 0% to 60% of the total flow. The ion-beam sputtering rate was 0.068 nm/s. For both sputtering methods, copper film thicknesses ranged from 2.5 to 100 nm. Films were deposited on 25 mm diameter glass substrates at a temperature of 298 K. An in-line four-point probe was used to measure sheet resistance.

The X-ray reflectivity measurements were conducted using Cu $K_{\alpha 1}$ radiation from a Rigaku ® RU300E rotating anode X-ray generator. Slits were used to define the beam size, which was 0.05 to 0.12 mm in the scattering plane and 4.0 mm out of the scattering plane. A 1 mm slit was used for collimation in the scattering plane[16]. The diffuse scattering background was subtracted from the raw data to yield the specular reflectivity.

Since the substrates were thin glass and tended to bow when held with our vacuum chuck holder, good reflectivity data could not be obtained for small incidence angles. Hence, only data for incidence angles above about 0.5 degrees were used for quantitative analysis. X-ray diffraction (XRD) was conducted at the National Synchrotron Light Source, beamline X20C, using 1 milliradian Soller slits for collimation[17] and a wavelength of 0.1203 nm. A grazing incidence geometry with an incident angle of 0.5 degrees was used to reduce background scattering from the glass substrate.

Rutherford backscattering spectrometry (RBS) specimens were 50 nm of Cu sputtered onto amorphous carbon substrates. RBS provided the oxygen composition of the Cu thin films to within a measurement uncertainty of 2 at%. The accelerator used for RBS was a National Electrostatics Corporation® 3UH Pelletron, in conjunction with a Si surface barrier charged particle detector. The primary He^+ ion beam was accelerated to an energy of 2.3 MeV with the detector at an angle of 170^o from the beam direction. RUMP® software was used to analyze the data using a second order polynomial fit to the square root of the energy.

III. RESISTIVITY MODELING

This section describes the models of electron transport commonly used to predict thin film conductivity. The extent to which conduction electrons scatter specularly from the interfaces of metal thin films has been a topic of research for over six decades. With the advent of spin-valve and other technologies, understanding and controlling specular reflection of electrons has gained practical importance. Electron conduction in fine-grained thin metal films is strongly influenced by surface roughness and grain size when

the film thickness approaches the mean free path of conduction electrons. Fuchs[18] and later Sondheimer[19] showed that the resistivity of thin alkali metal films increased with decreasing film thickness. Fuchs developed a model that accounts for both diffuse and elastic scattering of electrons at surfaces, includes the Fermi distribution function and considers a statistical distribution of electron mean free paths but does not take into account surface roughness. Sondheimer's and Fuchs' models are both semi-classical treatments based on Boltzmann transport theory and use a fixed specular reflection fraction that is independent of the angle of incidence of the electron with the surface.

Namba recognized the importance of the surface roughness in electron scattering, and building upon the Fuchs model, developed his model to simulate the surface roughness induced by grain boundaries. The widely accepted Fuchs-Namba model accounts for the surface roughness effect on conductivity.[20] Namba's model represents the surface roughness as a one-dimensional sinusoidal wave with a single peak-to-valley height. Namba's model does not consider the surface realistically as three-dimensional with a distribution of heights and lateral lengths and it does not account for grain boundary scattering. It assumes that the bulk resistivity, the electron mean free path and the roughness are independent of thickness.

Yamada *et al.*[21] applied the Fuchs-Namba model to *in-situ* sheet conductance vs. film thickness for ion-beam sputtered Co, Cu, $Ni_{80}Fe_{20}$, Ag and Ta films during growth and determined the specular reflection coefficient, bulk resistivity and roughness. They assumed the product of the bulk resistivity times the mean free path is constant for thin film materials. Atomic force microscopy (AFM) was used to measure surface roughness and it was observed that this surface roughness correlated well with the roughness

determined by the Fuchs-Namba model. The fitted specular reflection coefficients of the metal films ranged from 0 to 0.8, while the roughness ranged from 0.37 to 1.46 nm.

It is generally true that grain boundaries have a minor effect on the resistivities of bulk metals; however, for thin films, grain boundaries can play a dominant role. Mayadas and Shatzkes[22], by extending the Boltzmann transport theory, successfully accounted for the grain boundary reflection and transmission of electrons in polycrystalline thin metal films where the grain diameter approaches that of film thickness. Grain boundaries, acting as potential walls, were modeled as parallel planes oriented perpendicular to the direction of the current flow where the incident electrons are scattered. Some fraction of electrons is elastically reflected at the boundary (r) with the balance of electrons transmitted (1-r). The resulting resistivity is given by

$$\rho_{grain} = \rho_0 / \left[1 - (3/2)\alpha + 3\alpha^2 - 3\alpha^3 \ln(1 + 1/\alpha)\right] \qquad \text{[Eq. 1]}$$

where ρ_{grain} is grain boundary resistivity, ρ_o is bulk resistivity, D is grain diameter and $\alpha = \lambda r/(D(1-r))$ quantifies the importance of grain boundary scattering. Mayadas and Shatzkes[22] found that their model (Eq. 1) provided a good fit to resistivity data of evaporated thin Al films ranging in thickness from 100 to 1000 nm. They found that grain boundary scattering was the dominant mechanism for increased resistivity when the grain diameter was equal to or less than that of the electron mean-free-path. De Vries[23] studied room temperature evaporated films of Al, Co, Ni, Pd, Ag, and Au in thicknesses ranging from 10 to 300 nm. He related the dominance of grain boundary scattering to the increase in resistivity with decreasing film thickness.

Prior research highlights the problematic nature of attempting to account for all the factors that affect thin film resistivity,[18-20,23-25] because no model adequately accounts for

all effects due to inaccuracies introduced by the simplifying assumptions. It is understood now that the specular reflection of electrons at surfaces and grain boundaries, surface roughness, bulk resistivity, and mean free path are not independent of film thickness, grain diameter, crystalline texture, impurities, deposition temperature and deposition technique. Hence, some assumptions must be made in the resistivity data analysis.

In this paper we use a simplified version of Namba's model in our analysis:

$$\rho = \rho_0\left[1-(h/d)^2\right]^{-1/2} + \frac{3}{8d}\rho_0\lambda(1-P)\left[1-(h/d)^2\right]^{-3/2} \qquad \text{[Eq. 2]}$$

where ρ is film resistivity, d is film thickness, and h is peak-to-valley height of the sinusoidal roughness (i.e. grain grooves). The bulk resistivity (ρ_o), electron mean free path (λ) and roughness are assumed independent of thickness. The specular reflection factor, P, is the fraction of electrons that are reflected specularly at the interfaces and it varies from 1 for a perfectly reflective surface to 0 for a rough surface where electrons scatter diffusely. P accounts for the intrinsic properties of the two materials making the interface, but it is also has extrinsic components that are influenced by morphological effects of the interface such as small undulations not accounted for by the larger scale sinusoidal roughness (e.g., intermixing). Therefore, the specular reflection factor is dependent on film processing and may differ between the dc-magnetron and ion-beam sputtered films. Both the specular reflection coefficient and film roughness are assumed independent of thickness. The specular reflection coefficient and surface roughness are independent paramenters, as shown by the poor correlation between R and h in the study done by Vancea *et al*.[24] In modeling the data, the thin film bulk resistivity-mean free path product ($\rho_o\lambda$) is not the same as for the bulk material, and since it is not a material

constant, it is varied to increase the accuracy of the fit.[24,26] We also use the Mayadas-Shatzkes model (Eq. 1) to determine the effect of grain boundary scattering on bulk resistivity.

IV. RESULTS

A. Resistivity and Modeling

Figure 1 shows resistivity data with respect to oxygen concentration for the 4.5, 5.0, 10.0 and 100 nm films for the dc-magnetron (1(a)) and ion beam sputtered (1(b)) films. The bulk resistivity, approximated by that of the 100 nm films, is constant for the ion-beam films at concentration of < 10% O_2 before gradually increasing at concentrations >10% O_2, while in contrast, at only 0.2% O_2 the bulk resistivity of the dc-magnetron film begins sharply increasing above that for the unoxygenated films. For both deposition processes, the copper film resistivity increases with decreasing film thickness, as expected.[21] For films thinner than 10 nm, our dc-magnetron sputtered films decrease in resistivity as a function of O_2 reaching a minimum resistivity when the oxygen concentration was 0.2% to 1.0%, while for our ion-beam sputtered films, the addition of oxygen minimized the resistivity at oxygen concentrations of 6% to 10% (see Fig. 1). These results are in agreement with Egelhoff et al.[8], who reported a decrease in sheet resistance as a function of increasing film thicknesses (from 1 to 2.6 nm) at a 15% O_2 concentration in the sputtering atmosphere for dc-magnetron sputtered Co/Cu spin valves. These authors also found a pronounced drop in sheet resistance to a minimum at low oxygen pressures, followed by an increase at higher oxygen pressures in the sputtering atmosphere. The minimal resistivities of our dc-magnetron films are slightly higher than the minimal resistivities of our ion-beam films. For the 5 nm thick films, the

minimum resistivity was 32 μΩ–cm for dc-magnetron and 19 μΩ–cm for ion beam. Dc-magnetron requires roughly one tenth less oxygen, as a percentage of gas flow, in the sputtering atmosphere to minimize the copper resistivity when compared to ion beam. Less oxygen is required because the O_2 molecules readily dissociate in the high-energy plasma into reactive monoatomic oxygen, in contrast to the alternate pathway of surface mediated oxygen physisorption, dissociation, and chemisorption in ion-beam sputtering.[27] Both pathways provide oxygen to the growing surface.

The thickness dependence of the resistivity-thickness product (ρ x t) was analyzed using the Fuchs-Namba model, provided by Yamada,[21] to determine the bulk resistivity, roughness, and electron mean free path. Figure 2 shows the ρ x t-product as a function of thickness for the dc-magnetron films (2(a)) and for the ion-beam films (2(b)). Three trends are apparent from an examination of the figure. First, ρ x t increases sharply with decreasing thickness as surface and interface scattering of electrons dominates over bulk scattering. Eventually, the film is thin enough to become a continuous network of bridged islands that gives the highest resistivity. For thicknesses below this, the film is broken up into distinct islands, whereupon the resistivity becomes infinite. Second, the slope of the right hand portion of the curve, which represents the bulk resistivity, increases with O_2%. Third, the roughness, which is the approximate thickness where the resistivity begins to rapidly increase, is smaller for the dc-magnetron films sputtered in O_2 than for pure Cu magnetron films and for ion-beam films is smallest for films sputtered at 6-20% O_2.

The resistivity-thickness results of the Fuchs-Namba modeling are shown by the lines in Fig. 2 and, in most cases, model the data quite well. The modeling was done by first fixing P=0.5 and then incrementally adjusting the electron mean free path (MFP) to

minimize the goodness-of-fit (χ^2). The choice of P=0.5 results because P and the MFP are not independent (see Eq. 2) and for Cu P can range from 0.2 to 0.6.[21,28] The best fit values of MFP x P are presented in Figures 3(a) and 3(b) for dc-magnetron and ion-beam films, respectively. Figure 3(a) shows that for dc-magnetron films the MFP x P product decreases roughly exponentially with increasing oxygen. Figure 3(b) shows that for the ion-beam films in the oxygen concentration range from 2% to 10% the MFP x P product increases above that for 0% O_2; beyond 10% O_2 the MFP x P decreases with oxygen concentration. In ion-beam films sputtered in the O_2 range from 0% to 10% the MFP x P peak could be due to changes in both MFP and P, since these parameters are inseparable in this analysis. At least at the higher O_2 concentrations, for both film types, the ten-fold reduction of the MFP x P product is most likely driven by a significant reduction of the electron mean free path. This is an indication the atomic arrangement, electronic states, second phase impurities, or interface morphology of the films are altered by the presence of low concentrations of oxygen during sputtering, causing a measurable effect on electron scattering.

Figure 4 illustrates the root-mean-squared (rms) roughness ($h/(2\sqrt{2})$) calculated from fitting the Fuchs-Namba model and plotted as a function of oxygen concentration for the dc-magnetron and ion-beam films. The rms Fuchs-Namba roughness of the dc-magnetron sputtered copper/copper oxide interface is about 1.5 nm in the un-doped film and drops abruptly to a minimum around 0.85 nm at 0.6% to 2.0% O_2 before increasing back to about 1.5 nm for the highest doping levels of 3% O_2. The rms Fuchs-Namba roughness of the ion-beam sputtered copper/copper oxide interface is also 1.5 nm in the un-doped film, drops to a minimum around 1.0 nm at 6% to 10% O_2, then increases back

to about 1.35 nm for high concentrations. For both film types the Fuchs-Namba roughness reduction correlates with the O_2 concentration where the film resistivity is at a minimum and the absolute decrease of the surface roughness for both processing methods is similar.

In summary, for Cu films less than 5 nm thick 0.2% to 1% O_2 minimizes the resistivity of dc-magnetron sputtered films, while up to 6% to 10% O_2 is required to minimize the resistivity in ion-beam sputtered films. Greater O_2 concentrations beyond these levels result in higher resistivity. Films greater than 10 nm thick show a monotonic resistivity increase with O_2 concentration. The Fuchs-Namba modeling shows a significant reduction of the Cu interface roughness when sputtered in the presence of oxygen in the concentration range that minimized the resistivity.

B. Interface Roughness

Several methods were used to elucidate the microstructural differences between the dc-magnetron and ion-beam sputtered Cu films as a function of oxygen, with the results presented in the following three sections. X-ray reflectivity[16,17] was used to measure the film roughness, while X-ray diffraction (XRD) was used to identify the film phases, to quantify the Cu and Cu_2O grain sizes and to determine the concentration of the cuprous oxide in the films. RBS was used to determine the atomic oxygen concentration in the films.

X-ray reflectivity measurements of the interfacial roughness were made on 10 nm thick films, because this is near the optimal thickness for X-ray reflectivity and is close to the thickness of practical interest. To corroborate these results, we have also studied the

microstructure of 50 nm ion-beam Cu films grown under similar conditions and we find results consistent with those given below. Figure 5 shows reflectivity curves for four oxygen doping levels plotted as a function of the scattering vector $Q=(4\pi/\lambda)\sin\theta$, where λ is the X-ray wavelength and θ is the reflection angle. The film thickness determines the spacing between oscillation fringes, while the decay of the amplitude of the fringes with increasing Q is determined by the film roughness. For dc-magnetron sputtered films, the fringes extend to higher Q for the 1% and 2% oxygen film compared with the un-doped film (0.65 compared to 0.35 $Å^{-1}$, respectively), and hence the 1% O_2 film is smoothest, the 2% O_2 is the next smoothest, while the 0% O_2 film is the roughest. For ion-beam sputtered films, the fringes extend to higher Q for the 10% oxygen film compared with the un-doped film (0.5 compared to 0.4 $Å^{-1}$, respectively), and hence the 10% O_2 film is smoother than 0% O_2 film.

To quantify the film interface roughness, the reflectivity data were fit to a multilayer Parratt model[29] with two layers: Cu film and surface Cu oxide (shown below to be Cu_2O). The surface and Cu/Cu_2O roughnesses were fixed at the same value. The fits are shown by the lines in Figure 5 and adequately model the data. Figure 4 shows the rms Cu/Cu_2O interface roughness extracted from the fits as a function of oxygen concentration for both dc-magnetron (a) and ion-beam films (b). This shows that the rms roughness of the dc-magnetron sputtered copper/copper oxide interface is about 1.1 nm in the un-doped film, but drops to a minimum of 0.5 nm at 1.0% and 2.0% O_2. Second, the rms roughness of the ion-beam sputtered copper/copper oxide interface is 1.2 nm in the un-doped film, drops to a minimum of 0.7 nm at 6% to 10% O_2, then increases back to about 1.2 nm for high doping levels. The roughness minima, measured by X-ray

reflectivity, correlate well with the Fuchs-Namba calculated roughness minima, and both correlate with the resistivity minima.

C. Composition

This section describes how film composition was determined by X-ray diffraction and RBS measurements of the copper films. Figure 6 shows XRD data taken on 10 nm dc-magnetron and ion-beam sputtered Cu thin films, displaying intensity as a function of Q for several O_2 sputtering concentrations. It is apparent that Cu_2O is also present in the films and the diffraction peaks from Cu and Cu_2O are labeled. The most important point is that the widths of the copper (111), (200), and (220) peaks increase with increasing oxygen concentration. This shows that the Cu grain size decreases with oxygen atomic concentration and is further quantified below. There is Cu_2O present in the 0% O_2 films, which results from the thin, native surface oxide. We have estimated the Cu_2O atomic concentration from the ratio of the integrated intensities of the Cu (111) and the Cu_2O (111) Bragg peaks (normalized for the scattering strengths of Cu (111) and Cu_2O (111)). Since we are interested in the Cu_2O within the Cu film, we have subtracted the surface Cu_2O (obtained from the 0% film). Figure 7 shows the film cuprous oxide atomic concentration as a function of oxygen concentration for the two film types. The cuprous oxide concentration is large in dc-magnetron films for the range of 1.0% to 2.0 % O_2, while in ion-beam films the cuprous oxide concentration is small for <10% O_2, but increases significantly for >15% oxygen. In the low resistivity dc-magnetron films, the Cu_2O fraction is significantly larger than for low resistivity ion-beam films.

The atomic oxygen concentration from RBS was used to calculate the oxide fraction, based on the surface atomic density, assuming all oxygen in the film formed

stoichiometric Cu_2O. Plots of cuprous oxide as a function of sputtering gas oxygen concentration for the two film types are shown in Fig. 7, where we have subtracted the surface Cu_2O (obtained from the 0% film). As will be apparent, these data are consistent with the Cu_2O concentrations obtained from x-ray diffraction. For the dc-magnetron films (open symbols), the cuprous oxide concentration increases sharply, while for the ion-beam films (solid symbols), the cuprous oxide concentration is nearly constant (approximately 1%) up to about 10% O_2 concentration in the flow, and then begins to increase gradually. Cu films that have minimal resistivity contain cuprous oxide fractions ranging from 1.5% to 5.6% for dc-magnetron and 0.6% to 0.8% for ion-beam sputtering. The fact that the cuprous oxide concentration in the minimal resistivity dc-magnetron films is greater (by five to six times) than that of the minimal resistivity ion-beam films is not surprising given the resistance behavior.

From the Cu peak positions in XRD, we have calculated the average lateral Cu lattice parameters, which are shown in Fig. 8, for dc-magnetron and ion-beam films. These values are within 0.2% of the bulk value of 3.615 Å for an unstrained material[30]; they are independent of the Cu_2O concentration, to within the error bars (< 0.05%). This indicates that for all oxygen flow rates in both types of films there is no interstitial oxygen (<0.1 at.%), since this would significantly increase the lattice parameter; therefore, all oxygen is incorporated into the Cu as Cu_2O. This conclusion is supported by the good agreement between the Cu_2O fraction calculated from the RBS (which measures total oxygen) and XRD (which measures only the oxygen in Cu_2O) data (Fig. 7).

D. Grain Size

The film grain size was examined to gain a better understanding of how the film microstructure influences the interface roughness and resistivity. To determine the Cu and Cu_2O grain sizes, the XRD data were fit to a model where the diffraction peak shapes contain contributions from nonuniform strain and grain size broadening.[31] The nonuniform strain contribution (variation in lattice constant through the film) was assumed to have a Gaussian distribution, while the size broadening was assumed to originate from a log-normal distribution[32] of grain sizes using an approximation given by Popa and Balzar.[33] The fits to the diffraction data are shown by the lines in Fig. 6 and model the data quite well. Figure 9 shows the best-fit area-weighted average copper and cuprous oxide grain diameter as a function of oxygen concentration for the dc-magnetron and ion-beam films. This shows that the Cu grain diameter is significantly reduced by increasing oxygen concentration in the sputtering gas for both dc-magnetron and ion beam sputtering processes. The pure Cu grain diameter for the dc-magnetron sputtered films is approximately the same as for ion-beam films. However, the oxygen has a pronounced affect on reducing the dc-magnetron Cu grain size, which is consistent with the strong increase of bulk resistivity for the dc-magnetron films in Fig. 1. Similarly, at the respective oxygen concentrations that produce films with minimal resistivity, the dc-magnetron sputtered copper grains are 30% smaller than the ion-beam sputtered copper grains. The nanoscale Cu_2O particle diameter appears to be independent of oxygen concentration, and these grains are approximately the same size for dc-magnetron and ion-beam films (approximately 3 to 4 nm); recall that for low Cu_2O, the Cu_2O is all from the surface oxide.

Figure 10 shows bulk resistivity as a function of the cuprous oxide concentration in 10 nm films for both dc-magnetron and ion-beam deposition. The bulk resistivity comes from Fuchs-Namba modeling (approximately equal to ρ for 100 nm films), while the cuprous oxide concentration was calculated from XRD data assuming all the oxygen in the film is Cu_2O after subtracting off the surface oxide. The dependence of the data in Fig. 10 is due to both the increased presence of the non-conductive Cu_2O and to the decrease in Cu grain size with increasing Cu_2O (Fig. 9). To determine the dominant mechanism, the data were modeled with both a rule-of-mixtures[34] that accounts for the presence of a nonconductive second phase and a grain boundary scattering model. The grain boundary scattering of conduction electrons is given by the Mayadas-Shatzkes equation[22] [Eq. 1], assuming a constant value for bulk resistivity of 1.57 μΩ-cm (pure bulk Cu), grain boundary reflectivity of 0.4 used by Harper *et al.*[35], and a mean free path of 39 nm.[36] The grain diameter was taken from the XRD results in Fig. 9. The two models are shown by the lines in Fig. 10; they both show an increase in resistivity with increasing Cu_2O, but do not explain the data. Hence, while both the grain boundary scattering mechanism and the nonconductive second phase account for part of the bulk resistivity increase, some other mechanism must be operative. We suspect that significant scattering of conduction electrons off the nanoscale, second phase Cu_2O particles must be adequately addressed to explain the bulk resistivity increase of partially oxidized copper.

V. DISCUSSION

Our results shed light on the similarities and subtle differences between the mechanisms of resistivity reduction of partially oxygenated Cu films deposited by dc-

magnetron and ion-beam sputtering. Dc-magnetron deposition requires less oxygen in the sputtering atmosphere to produce films with minimal resistivity, but the films with minimum resistivity actually contain a much higher fraction of cuprous oxide in the film compared to ion-beam films. These more heavily oxidized dc-magnetron films, hence, have a higher bulk resistivity than ion-beam films. In both film types, the oxygen is incorporated as a Cu_2O phase and is not interstitial. Interface roughness is minimized in the O_2 range of 0.2% to 1.0% for dc-magnetron and 6% to 10% O_2 for ion-beam and the dc-magnetron interfaces are smoother. Cu grain sizes are reduced in the partially oxidized films, compared to the pure Cu films. The dc-magnetron Cu grain diameter is reduced by as much as 30% in the range of O_2 concentrations, in which both the resistivity and interface roughness were minimized. In contrast, the ion-beam films have only a 14% grain diameter reduction.

The Fuchs-Namba modeling and X-ray reflectivity measurements (Fig. 4) indicate that the sharp decrease in resistivity for both film types is due to similar roughness reduction at the interface between the Cu and the top film of Cu_2O. The smoothing we observe is similar to results seen by others[10] who sputtered Cu/Co films with in a partial oxygen atmosphere. We believe that the reduction in resistivity is due to improved reflection of conduction electrons off smoother interfaces. Electron scattering by the interface roughness is phenomenologically accounted for by the sinusoidal height (h) in (Eq. 2); a smooth surface (small h) is more reflective to incident electrons, while a rough surface (large h) is less reflective because it tends to scatter electrons along the curvature of the grain surfaces and at the grain grooves. These conclusions are in agreement with three-dimensional Monte Carlo simulations by Kuan *et al.*[36] that quantified the effects on

electron transport of electron trajectories off rough surfaces. They found the resistivity rise in Cu thin films was proportional to the amplitude of the surface roughness, which was supported by AFM and cross sectional TEM. These results indicate that surface roughness is a critical parameter that helps to reduce electron scattering and achieve low resistivity.

Thin film composition is an important parameter that strongly affected resistivity: it was controlled by the sputtering gas composition. The five to six times higher concentration of Cu_2O particles in the dc-magnetron Cu films is attributed to the generally ten times higher molecular oxygen flux. Based on the partial pressure of oxygen, for example, the O_2 flux in dc-magnetron sputtering is 6.45×10^{19} molecules/cm^2-sec (0.6% O_2), while in ion-beam sputtering it is 6.65×10^{18} molecules/cm^2-sec (10% O_2). We believe the higher concentration of nonconductive cuprous oxide particles increase diffuse electron scattering, which in part, explains the generally two to ten times higher resistivity measured on all thickness of the dc-magnetron films at O_2 concentrations of 0.6% and greater (compared to ion-beam); it is primarily responsible for the increase in bulk resistivity with respect to oxygen.

We find that the presence of oxygen results in a reduction in the film grain size for both deposition techniques. This is apparently in conflict with the larger grains proposed by Egelhoff *et al.*[9] for Co/Cu spin valves dc-magnetron sputtered in oxygen containing atmospheres, but this discrepancy may be related to the lower oxygen concentrations they used ($<1 \times 10^{-6}$ Pa). Although one expects that smaller grain films should have higher resistivity, due to more grain boundary scattering of the electrons, the drop in resistivity for the ion-beam and the dc-magnetron thin films (<10 nm) did not correlate to grain size.

The resistivity drop occurs because our polycrystalline films, composed of smaller grains, have smoother interfaces (see Fig. 3), which result in a reduced resistivity, consistent with the conclusion of Miura[10]. Hence, for our deposition conditions, oxygen is not acting as a surfactant to reduce grain boundary grooving; rather it forms nano-scale cuprous oxide particles that obstruct Cu grain growth. This is in agreement with pinning of grain boundaries by an array of fine particles composed of organic impurities: a mechanism proposed to explain abnormal grain growth in electroplated Cu.[35] This conclusion suggests that specular scattering of electrons off the smoother interface occurs in both fine grained dc-magnetron and ion-beam sputtered films. In the thinnest fine-grain films, it appears interface smoothing has a stronger effect on resistivity than grain boundary scattering; nevertheless, the finer grain dc-magnetron films have a somewhat larger grain boundary scattering component to resistivity. We find that dc-magnetron films have the same size grains for pure Cu compared to ion-beam films; Bailey *et al*[14] found ion-beam grains to be larger, possibly due to effects coming from the different seed layers used and the resulting growth mode variation.

These results are of particular interest because the thinnest Cu film thicknesses studied are similar to the spin-valve copper spacer layer thicknesses (2.4nm)[5] and are substantially less than the mean free path of the electron in Cu, which has been reported to range from 12.7 to 39.0 nm in thin films.[21,24,26,28,36] Partial oxidation has been demonstrated as a method to refine the grain size, smooth the interface of a Cu thin film, and reduce the Cu thin film resistivity.

VI. SUMMARY AND CONCLUSIONS

In summary, dc-magnetron and ion-beam sputtering of copper films in a partial atmosphere of oxygen are effective means to reduce Cu thin-film resistivity. Cu films produced by ion-beam sputtering are preferred because they have less Cu_2O and lower bulk resistivity. For films 5 nm and thinner, the resistivity of the Cu films is minimized at oxygen concentrations ranging from 0.2% to 1% for dc-magnetron sputtering and 6% to 10% for ion-beam sputtering. At these O_2 concentrations, there is strong correlation between the Fuchs-Namba calculated roughness and the Cu/Cu_2O interface roughness of 10 nm films measured by X-ray reflectivity. We believe that this roughness reduction leads to the decrease in resistivity through an increase in the specular electron scattering at the film interfaces. At these optimal O_2 concentrations, the cuprous oxide fraction in the dc-magnetron film is about six times greater that in the ion-beam sputtered film and the Cu grain size is refined in both. We attribute the grain refinement to the presence of nano-scale cuprous oxide particles disrupting the Cu grain growth, which produces a smooth specular interface that reflect electrons, thus lowering film resistivity.

ACKNOWLEDGEMENTS

This study was supported by IBM Almaden Research Center in conjunction with San José State University under National Science Foundation grant CHE-9625628 and with James Madison University under NSF GOALI grant CHE9625628. This research was carried out in part at the National Synchrotron Light Source, Brookhaven National Laboratory, which is supported by the U.S. Department of Energy, Division of Materials Sciences and Division of Chemical Sciences, under Contract No. DE-AC02-98CH10886. Portions of this research were carried out at the Stanford Synchrotron Radiation

Laboratory, a user facility operated by Stanford University on behalf of the U.S. Department of Energy, Office of Basic Energy Sciences. The guidance of Dr. R. Lawrence Comstock of San Jose State University is greatly appreciated.

References

1) R. L. Comstock, J. Mater. Sci.: Mater. Electron. **13,** 509 (2002).

2) J.F. Gregg, I. Petej, E. Jouguelet, C. Dennis, J. Phys. D: Appl. Phys. **35**, R121 (2002).

3) W. E. Bailey, C. Fery, K. Yamada, and S. X. Wang, J. Appl. Phys. **85(10)**, 7345 (1999).

4) S. X. Wang, K. Yamada, and W.E. Bailey, IEEE Trans. Magn. **36(5),** 2841 (2000).

5) W. Y. Lee, M. Carey, M. F. Toney, P. Rice, B. Gurney, H.-C. Chang, E. Allen, and D. Mauri, J. Appl. Phys. **89(11)**, 6925 (2001).

6) Z. Diao, Y. Huai, and L. Chen, J. Appl. Phys. **91(10)**, 7104 (2002).

7) A. Al-Jibouri, M. Hoban, Z. Lu, and G. Pan, J. Appl. Phys. **91(10)**, 7104 (2002).

8) W. F. Egelhoff, C.J. Powell, R.D. McMichael, and A.E. Berkowitz, J. Vac. Sci. Technol. B **17(4)**, 1702 (1999).

9) W. F. Egelhoff, P. J. Chen, C. J. Powell, M. D. Stiles, R. D. McMichael, J. H. Judy, K. Takano, and A. E. Berkowitz, J. Appl. Phys. **82(12)**, 6142 (1997).

10) S. Miura, M. Tsunoda, and M. Takahashi, J. Appl. Phys. **89(11)**, 6308 (2001).

11) D. J. Larson, A. K. Petford-Long, A. Cerezo, S. P. Bozeman, A. Morrone, Y. Q. Ma, A. Georgalakis, and P.H. Clifton, Phys. Rev. B **67**, 144420 (2003).

12) K. Li, G. Han, J. Qiu, P. Luo, Z. Guo, Y. Zheng, and Y. Wu, J. Appl. Phys. **93(10)**, 7708 (2003).

13) B. L. Peterson, R. L. White, and B. M. Clemens, Physica B **336**, 145 (2003).

14) W. E. Bailey, N.-C. Zhu, R. Sinclair, and S. X. Wang, J. Appl. Phys. **79(8)**, 6393 (1996).

15) W. L. Prater, E. L. Allen, W.-Y. Lee, M. F. Toney, J. Daniels, and J. A. Hedstrom, Appl. Phy. Let. **84(14)**, 2518 (2004).

16) C. M. Mate, B.K. Yen, D. C. Miller, M. F. Toney, M. Scarpulla, and J. E. Frommer, IEEE Trans. Magn. **36(1)**, 110 (2000).

17) M. F. Toney, W. Y. Lee, J. A. Hedstrom, and A. Kellock, J. Appl. Phys. **93(12)**, 9902 (2003).

18) K. Fuchs and H.H. Wills, Proc. Cambridge Philos. Soc. **34**, 100 (1938).

19) E. H. Sondheimer, Adv. Phys. **1,** 1 (1952).

20) Y. Namba, Jap. J. Appl. Phys. **9(11)**, 1326 (1970).

21) K. Yamada, W. E. Bailey, C. Fery, and S. X. Wang, IEEE Trans. Magn. **35(5)**, 2979 (1999).

22) A. F. Mayadas and M. Shatzkes, Phys. Rev. B **1(4),** 1382 (1970).

23) J. W. C. de Vries, Thin Solid Films, **167**, 25 (1988).

24) J. Vancea, H. Hoffmann, and K. Kastner, Thin Solid Films, **121**, 201 (1984).

25) H. Hoffmann and J. Vancea, Thin Solid Films, **85**, 147 (1981).

26) B. A. Gurney, V. S. Speriosu, J-P.Nozieres, H. Lefakis, D. R. Wilhoit, and O. U. Need, Phys. Rev. Let. **71(24)**, 4023 (1993).

27) D. L. Smith, *Thin-Film Deposition Principles and Practice* (McGraw-Hill, San Francisco, CA, 1995).

28) Th. Eckl, G. Reiss, H. Bruckl, and H. Hoffman, J. Appl. Phys. **75(1),** 362 (1992).

29) V. Holy, U. Pietsch, and T. Baumbach, *High resolution X-ray Scattering from Thin Films and Multilayers* (Springer, Berlin, 1992).

30) B. D. Cullity, *Elements of X-ray Diffraction* 3rd ed. (Prentice Hall, Upper Saddle River, NJ, 2001).

31) B. E. Warren, *X-ray Diffraction* (Dover Publications, Reading, MA., 1969).

32) J. Heintzenberg, Aerosol Sci. Techn. **21**, 46 (1994).

33) N. C. Popa and D. Balzar, J. Appl. Cryst. **35**, 338 (2002).

34) S. O. Kasap, *Principles of Electrical Engineering Materials and Devices* rev. ed. McGraw-Hill, San Francisco, CA, 2000).

35) J. M. E. Harper, C. Cabral, P.C. Andriacacos, L. Gignac, I.C. Noyan, K. P. Rodbell, and C. K. Hu, J. Appl. Phys. **86(5),** 2516 (1999).

36) T. S. Kuan, C. K. Inoki, G. S. Oehrlein, K. Rose, Y.-P. Zhao, G.-C. Wang, S.M. Rossnagle, and C. Cabral, Mat. Res. Soc. Symp. Proc. **612**, D7.1.1 (2000).

Figure Captions

FIG. 1. Cu film resistivity as a function of volumetric oxygen concentration during sputtering for dc-magnetron (a) and ion-beam (b) deposition for four different film thicknesses. The lines serve as guides to the eye.

FIG. 2. Points show resistivity x thickness vs. thickness data for Cu film deposited by dc-magnetron and ion-beam sputtering, (a) and (b), respectively. The lines show the Fuchs-Namba model fits to the data.

FIG 3. Electron MFP x P product as a function of volumetric oxygen concentration for dc-magnetron (a) and ion-beam deposition (b). Lines serve as guides for the eye.

FIG. 4. Interface roughness of 10 nm Cu as a function of volumetric oxygen concentration during sputtering. Solid and open symbols represent ion-beam and dc-magnetron data, respectively. Solid lines are guides for x-ray reflectivity roughness measurements and dashed lines are guides for roughness determined by the Fuchs-Namba model (F-N).

FIG. 5. X-ray reflectivity data for 10 nm dc-magnetron sputtered Cu films with 0, 1 and 2% O_2 (a) and for 10 nm ion-beam sputtered Cu films with 0, 6, 10 and 30% O_2 (b). Lines are fits to the data. For clarity, the curves are offset along the vertical axis.

FIG. 6. X-ray diffraction of 10 nm dc-magnetron sputtered Cu films with three different O_2 volumetric concentrations (a) and 10 nm ion-beam sputtered Cu films with five

different O_2 volumetric concentrations (b); Miller indices identify the Bragg peaks. Solid lines are fits to the data. For clarity, each curve is offset along the vertical axis.

FIG. 7. Cu film atomic composition as a function of volumetric oxygen concentration during sputtering. Solid and open symbols represent ion-beam and dc-magnetron, respectively. Lines serve as guides for the eye.

FIG. 8. Cu lattice constant as a function of cuprous oxide atomic concentration during sputtering in 10 nm films. Diamonds and squares represent dc-magnetron and ion-beam, respectively.

FIG. 9. Area-weighted average grain diameter as a function of volumetric oxygen concentration during sputtering for 10 nm films. Solid and open symbols represent ion-beam and dc-magnetron, respectively. Cu data are shown as solid lines, while cuprous oxide data are shown as a dashed line, which serve as guides for the eye.

FIG. 10. Bulk resistivity as a function of Cu_2O atomic fraction for dc-magnetron (diamonds) and ion-beam (squares). The solid line is the resistivity estimate from the Mayadas-Shatzkes model of grain boundary scattering, while the dashed lines is the resistivity from second phase scattering based on the rule-of-mixtures.

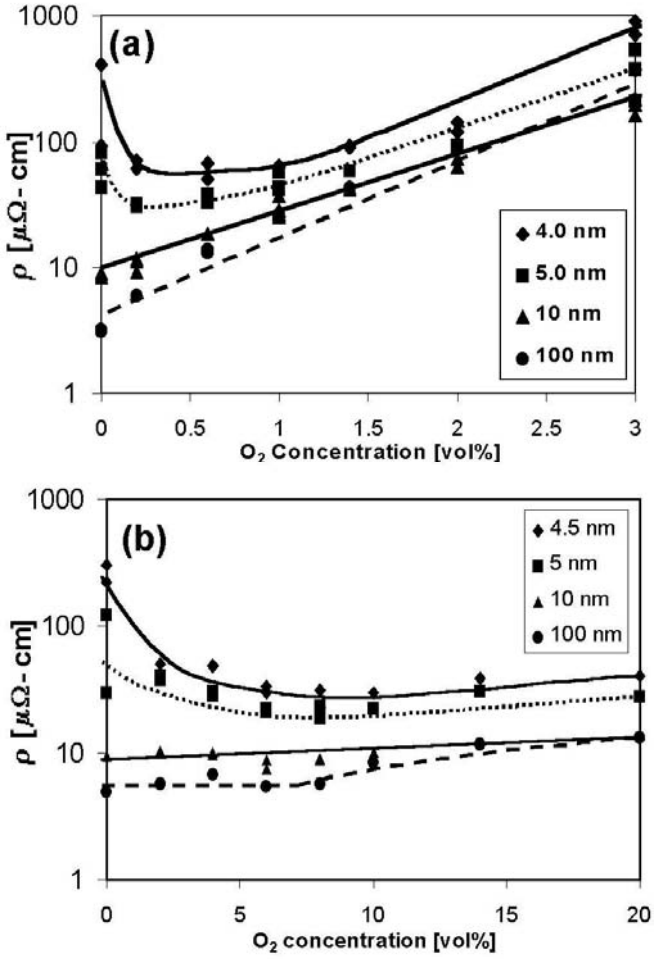

JAP JR04-1621 Figure 1 by Prater *et al.*

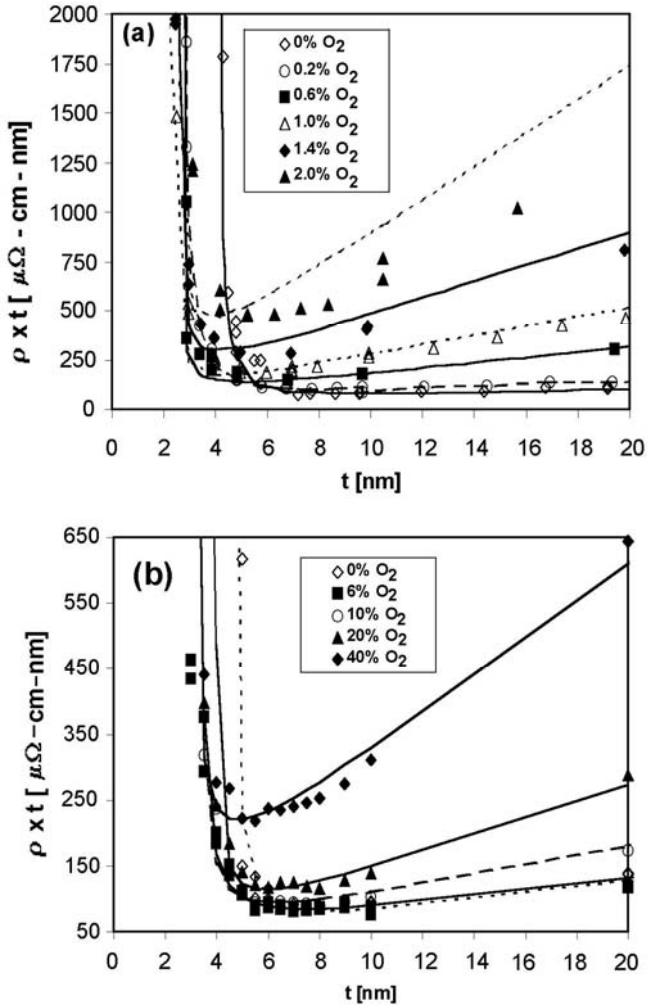

JAP JR04-1621 Figure 2 by Prater *et al.*

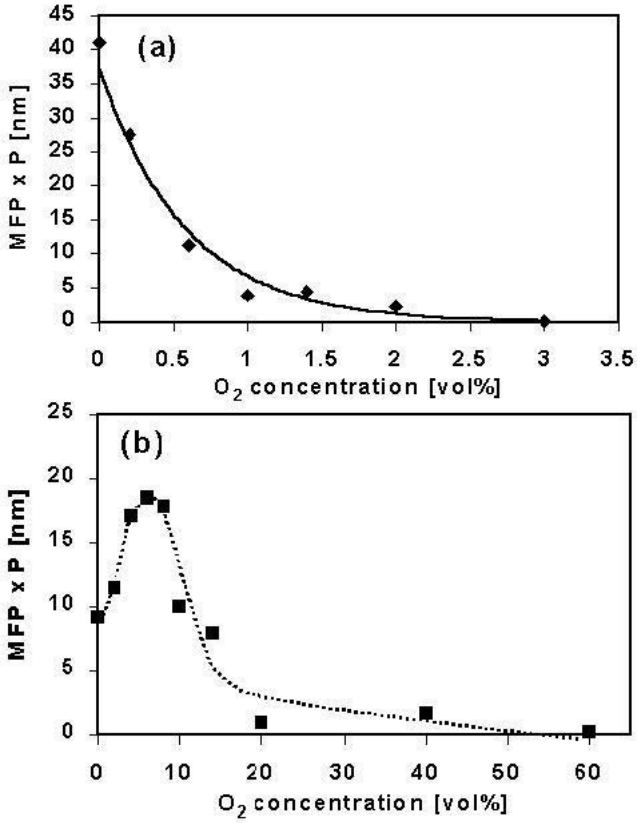

JAP JR04-1621 Figure 3 by Prater *et al.*

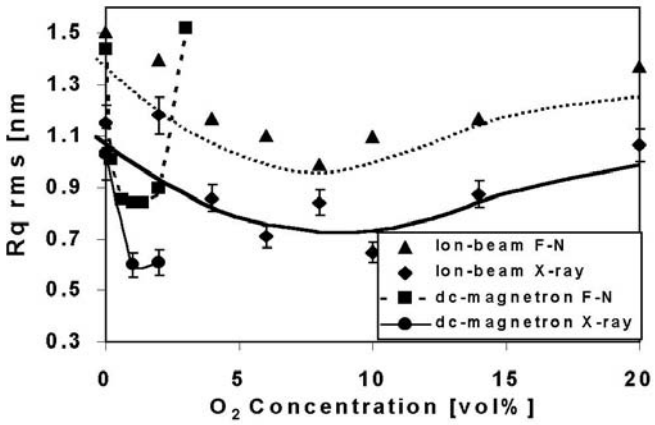

JAP JR04-1621 Figure 4 by Prater *et al*.

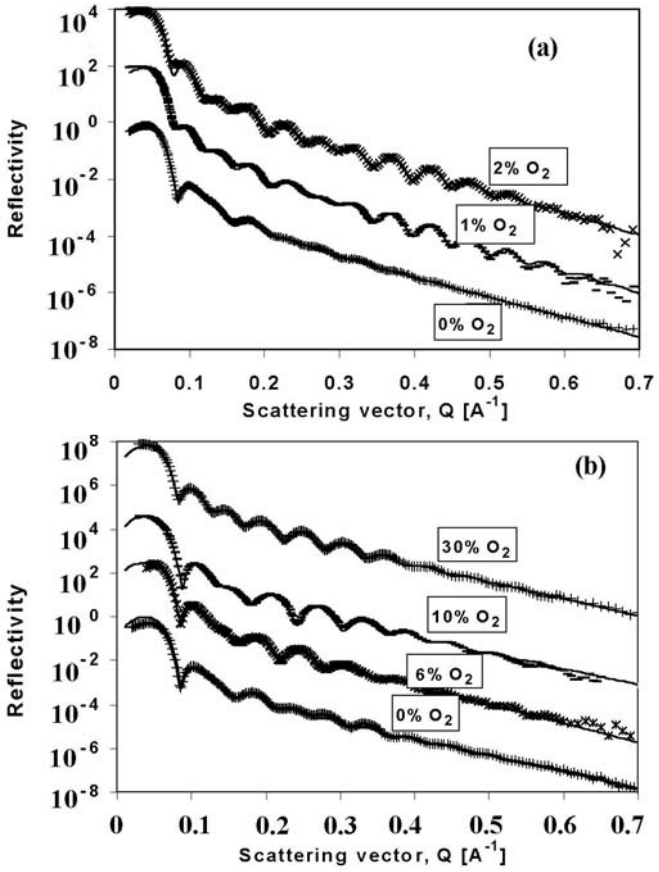

JAP JR04-1621 Figure 5 by Prater *et al*

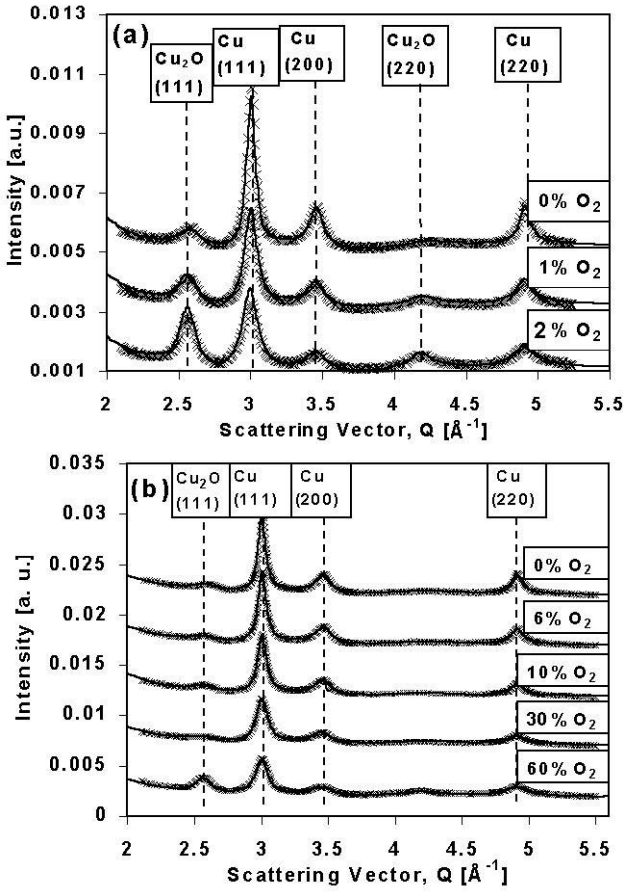

JAP JR04-1621 Figure 6 by Prater *et al.*

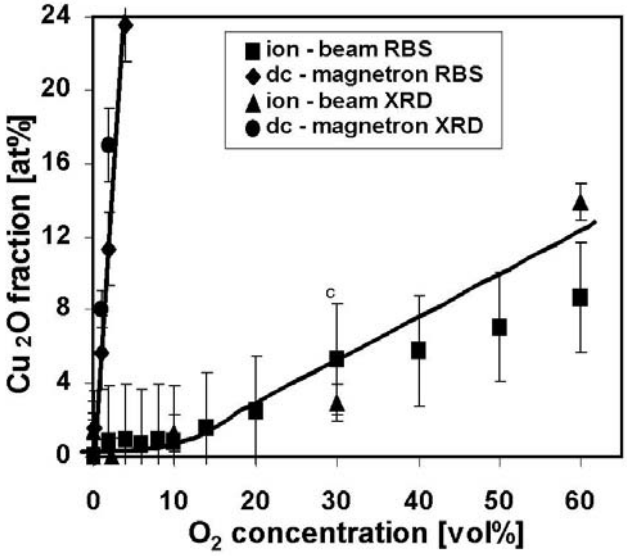

JAP JR04-1621 Figure 7 by Prater *et al*.

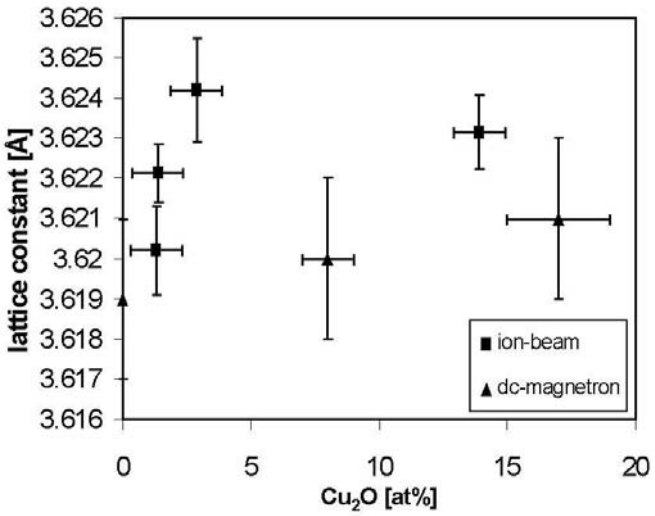

JAP JR04-1621 Figure 8 by Prater *et al*.

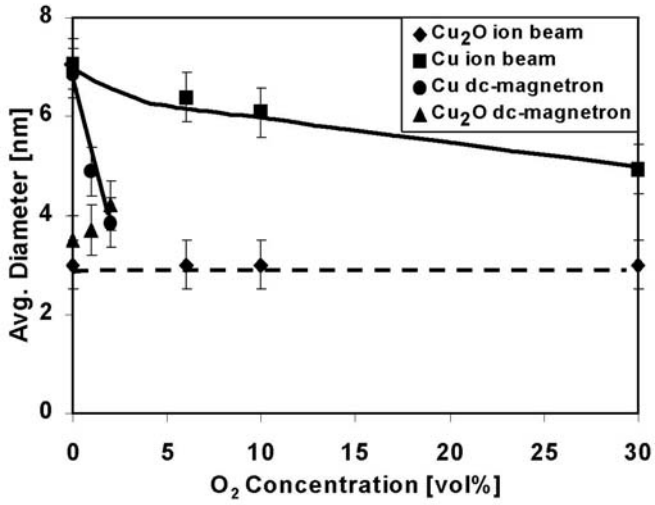

JAP JR04-1621 Figure 9 by Prater *et al.*

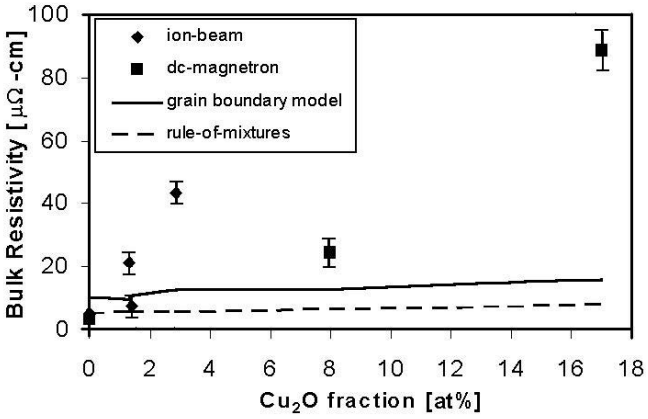

JAP JR04-1621 Figure 10 by Prater *et al.*